Applied Energy 119 (2014) 351–362

Contents lists available at ScienceDirect

Applied Energy

journal homepage: www.elsevier.com/locate/apenergy

Modelling of a chemisorption refrigeration and power cogeneration system

Huashan Bao *, Yaodong Wang, Anthony Paul Roskilly [1]

Sir Joseph Swan Centre for Energy Research, Newcastle University, Newcastle upon Tyne NE1 7RU, UK

HIGHLIGHTS

- An adsorption cogeneration was proposed and simulated for cooling and electricity.
- A dynamic model was built and studied to demonstrate the variability of the system.
- A dynamic model included the complex coupling of thermodynamic and chemical kinetic.
- Mutual constrains between main components and optimisation methods were discussed.
- The highest theoretical COP and exergy efficiency of cogeneration is 0.57 and 0.62.

ARTICLE INFO

Article history:
Received 3 June 2013
Received in revised form 5 December 2013
Accepted 6 January 2014

Keywords:
Cogeneration
Chemisorption
Scroll expander
Numerical modelling
Power generation
Refrigeration

ABSTRACT

The present work for the first time explores the possibility of a small-scale cogeneration unit by combining solid–gas chemisorption refrigeration cycle and a scroll expander. The innovation in this work is the capability of producing refrigeration and electricity continuously and simultaneously without aggravating the energy scarcity and environmental impact. Individual modelling for each component, which has been validated by experimental data, was firstly investigated in order to identify the proper operation condition for the cogeneration mode achieving 1000 W power output. Subsequently, with the integrated modelling of two components the cogeneration performance was studied to demonstrate the viability of this concept. However, because of the mutual constraint between the chemisorption and the expansion when they link in series, the power output of the cogeneration mode was only around one third of the original expectation under the same condition identified in the individual modelling. Methods of improving the global performance including the selection of reactive mediums were also discussed and would be of referable value for the future practical investigation.

1. Introduction

The Digest of United Kingdom Energy Statistics (DUKES) has estimated that over 80% and 30% of the demand for coal and natural gas, respectively, have been from major power producers over the last decade, which meanwhile is responsible for about one-quarter of total CO_2 emission in UK [1]. The dominated final electricity consumer in UK has been always the residential sector, the consumption of which increased by 58% between 1970 and 2011 [1]. More than 7% of total electricity generation has been lost through the transmission and distribution system in UK, and surprisingly this figure is higher than that of other major European countries those have even lower population density, such as Spain, France and Germany [2]. Therefore, with the pressure to reduce fuel demand, to cut greenhouse gas emissions by 80% comparing to the level of 1990 by 2050 [3] and also to minimise the transmission and distribution losses, the domestic small-scale, distributed electric generators are required to assist households to reduce the carbon footprint of their homes.

There is increasing number of the domestic small-scale electric power generation systems ($\leqslant$6 kW) around the world employing renewable energy resources, like wind turbines, solar panels, hydro turbines, geothermal heat, etc. [4]. Among those the cogeneration or tri-generation system (such as CCHP, combined cooling, heat and power) which yields multi-product to meet the daily demand of the average household are fairly attractive due to the further strengthened energy utilisation efficiency. For cogeneration of cooling and electricity or even CCHP, thermally driven refrigeration like absorption/adsorption is always one of the important technical strategies, where the ammonia as the working medium has been extensively engaged with thanks to its desirable characteristics of superior thermodynamic qualities, zero ODP and zero GWP.

* Corresponding author. Tel.: +44 001912464849.
E-mail addresses: huashan.bao@ncl.ac.uk (H. Bao), yaodong.wang@ncl.ac.uk (Y. Wang), tony.roskilly@ncl.ac.uk (A.P. Roskilly).
[1] Tel.: +44 191 208 5869; fax: +44 191 208 8533.

0306-2619/$ - see front matter © 2014 Elsevier Ltd. All rights reserved.
http://dx.doi.org/10.1016/j.apenergy.2014.01.012

Nomenclature

A	area (m^2)
C_a, C_r	axial, radial clearance (m)
COP	coefficient of performance (–)
c_p	heat capacity (J/kg/K)
F_t	force (N)
f_a, f_r	axial, radial flow coefficient (–)
f_{EG}	mass fraction (–)
H	height (m)
ΔH_r	reaction heat (J/mol (NH_3))
h	heat transfer coefficient ($W/m^2/K$)
h	enthalpy (J/kg)
$\hat{h}$	specific enthalpy on a molar basis (J/mol)
I	armature current (A)
J_s, J_L	moment of inertia of scroll and load (kg m^2)
k	expansion index (–)
k_s, k_L	friction coefficient of scroll and load (kg m^2/s)
k_e	coefficient of back electromotive force (V s/rad)
k_t	coefficient of torque sensitivity (N m/A)
L_a	axial clearance length (m)
L_{ar}	armature inductance (H)
m	mass (kg)
M	molar mass (kg/mol)
M_t	driving torque (N m)
$\dot{m}$	mass flow rate (kg/s)
n	molar number (mol)
P	pressure (Pa)
P_{it}	scroll pitch (m)
Power	power (W)
Q	heat (J)
r	basic circle radius (m)
R	resistance (Ω)
R_C	gas constant (J/mol/K)
R_{or}	orbiting radius (m)
t	time (s)
t_w	wrap thickness (m)
T	temperature (K)
T_L	load torque (N m)
UA	overall heat exchange coefficient (W/K)
V	volume (m^3)
W	work (W)
x	reaction conversion (–)
$[X]$	molar volumetric concentration (mol/m^3)

Greek letters

α	initial angle of involute
δ	thickness (m)
ε	porosity (–)
ε'	pressure ratio (–)
η	efficiency (-)
θ	rotation angle (rad)
λ	thermal conductivity (W/m/K)
v	molar volume (m^3/mol)
ρ	density (kg/m^3)
ω	angular velocity (rad/s)

Subscripts

a	axial
ar	armature
EG	expanded graphite
b	bulk
c	constraint
des	desorption
eq	equilibrium
ex	exergy
f	fluid
i	chamber number
in	inlet
L	load
mech	mechanical
out	outlet
r	reactant
ref	refrigeration
s	salt
shaft	shaft
syn	synthesis
S2	$MnCl_2{\cdot}2NH_3$
s6	$MnCl_2{\cdot}6NH_3$
tec	technical
therm	thermal
w	wall

Moreover, from an economic perspective, ammonia refrigeration is the most cost effective and energy efficient method of processing and storing frozen and unfrozen foods. Although ammonia is poisonous and flammable in high concentrations, two factors mitigate this risk: its distinctive smell is detectable at concentrations well below those considered to be dangerous, and ammonia is lighter than air, it will rise and dissipate in the atmosphere on its leakage. Various of well-recognised organisations such as BREEAM (Building Research Establishment Environmental Assessment Method, UK), UNEP (The United Nations Environmental Programme), and ASHRAE (American Society of Heating, Refrigerating and Air-Conditioning Engineers, Inc.). have given decent credits to ammonia and been promoting a variety of programs to preserve the economic benefits of ammonia refrigeration while providing for the management of risks [5].

An absorption cogeneration cycle producing cooling and electric power simultaneously was proposed by Goswami in 1995 [6]. Goswami cycle employs the binary mixture of ammonia and water as the working fluid and the rich-ammonia solution from the rectifier expands through a turbine, which is supposed to exit the turbine with a cold temperature and that is how it generates refrigeration. Hasan et al. [7] numerically analysed the energy and exergy efficiency of this cycle, and concluded that solar thermal energy at 77 °C could achieve an exergy efficiency higher than 0.6, the thermal efficiency of refrigeration and power generation with 127 °C heat source were 0.01 and 0.15, respectively. As a matter of fact, in realistic situation the cooling capacity probably would be much lower or even null as it could be attributed to the fact that at the exit of the turbine the rich ammonia binary mixture likely remains as wet vapour, rather than at liquid state to be vaporising for refrigeration [8].

Ammonia absorption power/cooling (APC) combined cycle emerged later as an improved cycle by employing a throttle valve to ensure the sub-cooling state before vaporisation. However, the complex design of APC cycle undoubtedly compromises the compactness of the system. Meanwhile it arouses the balance matching issue between the power output and the cooling load [9,10]. The thermal efficiency of cooling and net power reported by Liu and

Zhang [9] was numerically investigated with around 450 °C heat source and was presented as 0.06 and 0.21, respectively, while the exergy efficiency was around 0.58.

This work proposes a new concept of cooling and power simultaneous generation—adsorption cogeneration cycle (Ad-Cogen cycle), aimed to take full advantage of the merits of adsorption technology over absorption to promote the cogeneration idea. Such a cycle can be applied to small-scale household unit driven by solar energy, alternatively it can be designed for medium or large cogeneration plant using industrial waste heat. Since adsorption generously provides extended utilisation domain of thermal energy, from 50 °C to 600 °C, covering that of Goswami (80–150 °C) and APC (200–450 °C) cycles, it is convenient to select different suitable reactive candidates for different application circumstances. Adsorption system possesses a much simpler construction requiring easier operation and maintenance than that of absorption, such as no need of a liquid pump or rectifier or separator for refrigerant and no presence of crystallization problems [11–13]. The Ad-Cogen cycle theoretically embraces brighter prospect of cogeneration over Goswami cycle especially in term of refrigeration. This is partially because of the uncertainty of the exhausted working fluid from the expander in Goswami cycle as aforementioned. The refrigeration efficiency of the Ad-Cogen cycle ideally could be expected around 0.4. Moreover, the inherent intermittence of adsorption could mitigate the negative interplay between the power generation phase and the cooling producing phase in a complete two-phase cogeneration cycle to assure that vaporisation refrigeration starts off with adequately liquid working fluid. Besides, the intermittence favours the energy storage and better energy management. Considering these virtues of adsorption, it should be encouraged to explore the exciting potential of Ad-Cogen system. However, since the pure theoretical thermodynamic analysis of a resorption cogeneration system by Wang et al. [14] up to date there has been no publicly available report or publication studying on dynamic modelling or experimental investigation of such a cogeneration system yet. The presented work has for the first time carried out the numerical modelling study on an Ad-Cogen prototype to demonstrate the system viability and to probe the influential elements on the system performance. In order to further seek better knowledge for global system design and optimisation, this work was also studying the preferable operation conditions and the selection of the reactive salt complexes used in chemisorption part.

2. System design

As the principle of Ad-Cogen system being illustrated in Figs. 1 and 2 associated with the Clausius–Clapeyron diagram, one complete Ad-Cogen cycle can be depicted in two steps with a short period of intermission:

(1) In the first step (E–A–B), the Adsorbent Bed (Ad-Bed) receives Q_{des} from external high temperature heat source. Endothermic decomposition of the salt complex occurs once the thermodynamic properties of it deviates from the equilibrium line to some extent; at the same time the refrigerant is desorbed at vapour state with high temperature and high pressure and heads to the Expander for work output (W_{out}, A–B), or for the electric power output if there is a generator attached with the expander.

(2) Subsequently as the process B–C indicates the exhausted refrigerant from expander is collected and cooled down in the condenser simultaneously releasing Q_{cond} to the ambient and point C represents the saturated state of the refrigerant at heat sink temperature of 20 °C; afterwards, before the next step starts the liquid refrigerant transfers from the condenser to the evaporator awaiting vaporisation.

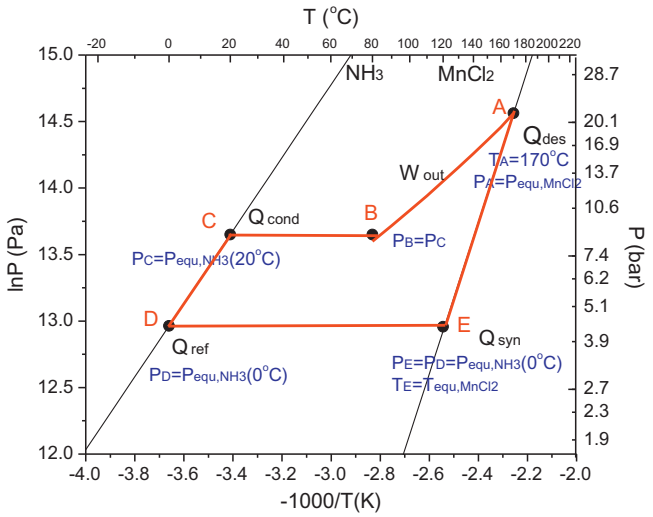

Fig. 1. P–T diagram of $MnCl_2/NH_3$ Ad-Cogen cycle.

(3) In the next step (C–D–E), the Ad-Bed is subjected to isobaric cooling at heat sink temperature (20 °C) in order to regain the adsorption ability; as soon as the thermodynamic properties of the reactive medium achieves a certain degree of the equilibrium drop (equilibrium temperature drop or pressure drop depending on the research preference) [15–17] which is the main force driving the chemical reaction, exothermal synthesis of the salt complex occurs associated with releasing heat Q_{syn}. Meanwhile, the refrigerant vaporises in the evaporator and extracts Q_{ref} from heat exchange medium at low temperature T_D (0 °C represented in Fig. 1), consequently producing cooling effect. Point D represents the saturated state of the refrigerant at refrigeration temperature; point E stands for the thermodynamic equilibrium state of the salt complex.

The presented Ad-Cogen system prototype comprises with two sets of the chemisorption cycle and a scroll expander for continuous and simultaneous cooling and power generation. Therefore, the two sub-Ad-Cogen sets jointly operate out of phase and promote the system performance as Fig. 2 illustrates. In Fig. 2(a), when Ad-Bed 1 undergoes desorption cycle and supplies the expander with vapour refrigerant for work output, Ad-Bed 2 extracts refrigerant from evaporator yielding refrigeration; in the next cycle, as shown in Fig. 2(b), switch the valves and swap the hot and cooling heat exchange fluids, thus the Ad-Bed 1 inversely has adsorption and Ad-Bed 2 runs desorption. Likewise, it keeps alternately recurring.

The reactants are $MnCl_2$ and ammonia as the adsorbent salt and the adsorbate refrigerant, respectively, the following reversible reaction occurs if the thermodynamic equilibrium drop is created.

$$MnCl_2 \cdot 2NH_3 + 4NH_3 = MnCl_2 \cdot 6NH_3 + 4\Delta H_r \quad (1)$$

3. Simulation modelling and analysis methods

The study route to accomplish the goal was following steps as below:

Firstly, a dynamic modelling of a scroll expander was established and examined. The simulation result then was compared with experimental data those were either from other published researches or from the practical tests by the authors. After the modelling being adjusted until good agreement achieved between

simulation and experiments, the expander modelling was simulated with the working fluid supplied by the chemisorption, and its specific conditions were identified to satisfy the demand of 1000 W power output.

Secondly, a dynamic modelling of adsorption cycle was created and studied independently of the expander. After the model validation with experimental data, the operating scenario of the chemisorption cycle was adjusted to meet the performance requirement of the expander, and then the dimension size of it was determined as its capacity was thereby predicted.

Finally, the coupling-performance of the two components as a whole cogeneration system was evaluated through the combination of two validated modelling. It is worth noting that the chemisorption is endowed with distinguished dynamic characteristics associated with chemical reaction kinetics, therefore the stationary modelling which considers the constant inputs and outputs of power generation with an empirical isentropic efficiency is inapplicable to the current circumstances. Afterwards, the influence factors on the overall performance were investigated by comparing and discussing the independently individual performance and cooperative performance of the two main components.

3.1. Adsorption cycle model

3.1.1. Kinetic model

The analogical model as expressed in Eqs. (2) and (3) were chosen respectively for decomposition and synthesis [15] in this work due to the limited information about the granulometric repartition, porosity, and inter- and intra- granular diffusivity of the composite of the expanded graphite impregnated with $MnCl_2$ complex. Unlike phenomenological kinetics describing the deeper mechanisms involved in the reaction, the analogical models consider more about the overall effect in a global way and they treat the presence of the different materials as an equivalent single entity, which in this work is a compound of the reactive ammoniates and the inert expanded graphite.

$$\frac{dx}{dt} = \mathrm{Ar}\cdot x^{\mathrm{Mr}}\cdot\frac{P_c - P_{eq}(T)}{P_c} \tag{2}$$

$$\frac{dx}{dt} = \mathrm{Ar}\cdot (1-x)^{\mathrm{Mr}}\cdot\frac{P_c - P_{eq}(T)}{P_c} \tag{3}$$

where x is the conversion rate of the reaction, which is ideally assumed in the range of 1–0 during decomposition (Eq. (2)) and from 0 to 1 during synthesis (Eq. (3)). Ar, the Affhenius factor, indicates the correlation between the reaction velocity and the working temperature. It was regarded as a constant coefficient in the current model. The exponential term Mr reflects the influence of the vacant sites on the reaction progress [18]. Ar and Mr for $MnCl_2$-ammonia reaction were suggested by Han et al. as 0.001087 and 1.185 respectively [15]. P_{eq} is the thermodynamic equilibrium pressure corresponding with the transient working temperature; P_c is the practical constraining working pressure.

For a single chemisorption cycle, P_c in the decomposition process was considered to be equal to the condensation pressure as the Ad-Bed being directly connected with the condenser. The Ad-Cogen system has the expander located in-between the Ad-Bed and the condenser, in this instance P_c of the decomposition equalled to the pressure in the suction chamber of the expander.

3.1.2. Heat transfer model

Fig. 3 shows the schematic diagram of the heat transfer model in the Ad-Bed. Although finned pipe type containers or other cylindrical containers may commonly be used as the Ad-bed, rectangular coordinate was employed in the present paper to simplify the model which more focuses on global phenomena. Lumped capacitance model was applied to the three components involved in the heat transfer, including the heat transfer fluid, the metallic container wall and the reactive mixture.

The governing equations describing the energy balance of all components are given as Eqs. (4)–(6).

$$m_f c_{pf}\frac{\partial T_f}{\partial t} = \dot{m}_f c_{pf}(T_{f,in} - T_{f,out}) - (UA)_{fw}\Delta T_{fw} \tag{4}$$

$$m_w c_{pw}\frac{\partial T_w}{\partial t} = (UA)_{fw}\Delta T_{fw} - (UA)_{wr}(T_w - T_r) \tag{5}$$

$$\left(\sum_{i=1}^{4} m_i c_{p,i}\right)\frac{\partial T_r}{\partial t} - m_{NH_3}\Delta H_r\frac{dx}{dt} = (UA)_{wr}(T_w - T_r) \tag{6}$$

Considering the turbulent flow inside the heat exchanger, there was a large value of the heat transfer coefficient between the heat exchange fluid and the container wall, which is the thin metallic wall of the Ad-Bed with high thermal conductivity. To simplify

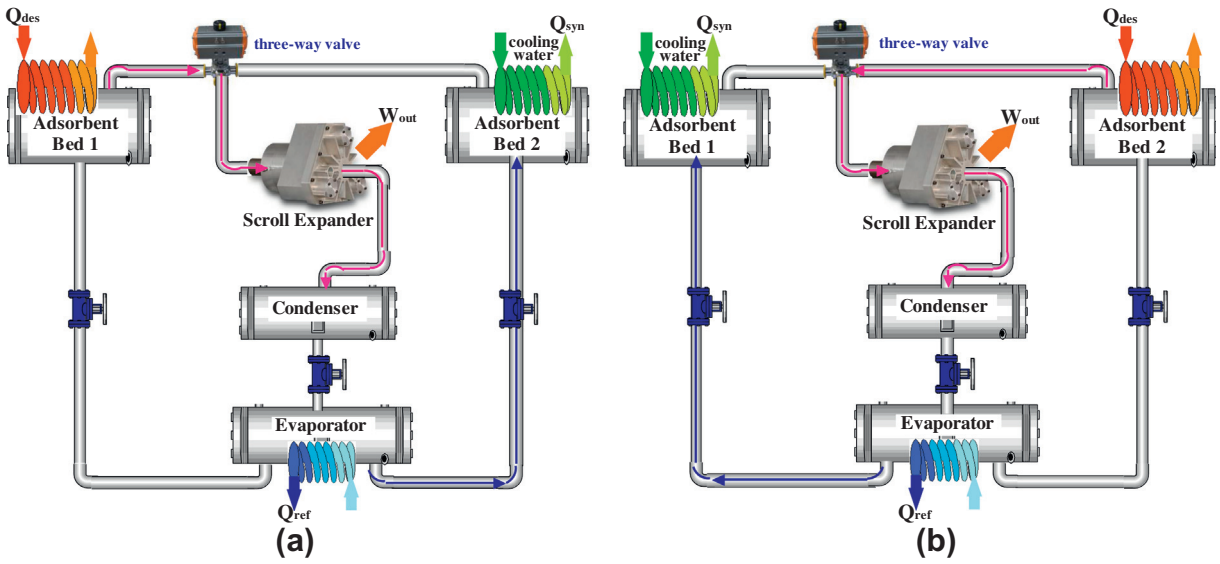

Fig. 2. Schematic of Ad-Cogen system in two consecutive cycles, (a) Ad-Bed 1 desorption, Ad-Bed 2 adsorption and (b) Ad-Bed 1 adsorption, Ad-Bed 2 desorption.

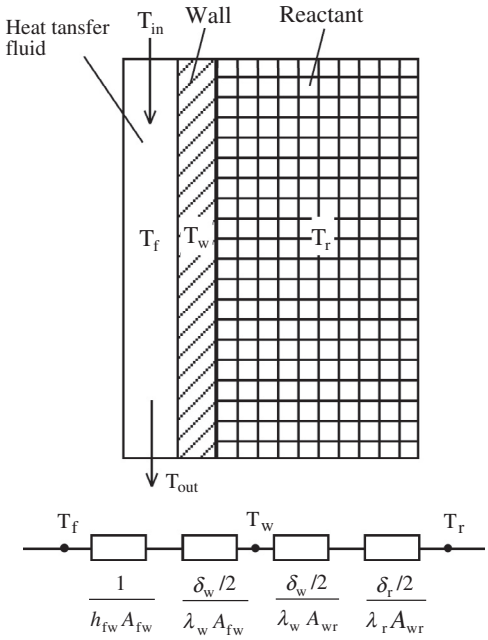

Fig. 3. Heat transfer in the reaction bed.

the model and to enhance the general applicability of the modelling, an approximation is applied which lumps the thermal mass of the heat transfer fluid inside the flow channel with the wall and treat them as a single element, though there is temperature difference between them [19]. Then Eqs. (4) and (5) become to the following equations.

$$\dot{m}_f c_{pf}(T_{f,in} - T_{f,out}) = (UA)_{fw}\Delta T_{fw} \tag{7}$$

$$(m_w c_{pw} + m_f c_{pf})\frac{\partial T_w}{\partial t} = \dot{m}_f c_{pf}(T_{f,in} - T_{f,out}) - (UA)_{wr}(T_w - T_r) \tag{8}$$

ΔT_{fw} is the log-mean temperature difference between the heat transfer fluid and the wall, which can be calculated by Eq. (9). The overall heat exchange coefficient $(UA)_{fw}$ between the heat transfer fluids and the container wall and $(UA)_{wr}$ between the container wall and reactive mixtures are expressed in Eqs. (10) and (11), respectively.

$$\Delta T_{fw} = \frac{T_{in} - T_{out}}{\ln\left(\frac{T_{in}-T_w}{T_{out}-T_w}\right)} \tag{9}$$

$$\frac{1}{(UA)_{fw}} = \frac{1}{h_{fw}A_{fw}} + \frac{\delta_w/2}{\lambda_w A_{fw}} \tag{10}$$

$$\frac{1}{(UA)_{wr}} = \frac{\delta_w/2}{\lambda_w A_{wr}} + \frac{\delta_r/2}{\lambda_r A_{wr}} \tag{11}$$

The heat capacity of the adsorbent mixture was calculated by Eq. (12), considering the contribution of the expanded graphite (EG), the refrigerant (NH_3) and the different $MnCl_2$ ammoniates (s2 denotes $MnCl_2{\cdot}2NH_3$ and s6 for $MnCl_2{\cdot}6NH_3$) those might exist simultaneously; the porosity of the adsorbent compound block was obtained with Eq. (13).

$$\begin{aligned}\sum_{i=1}^{4}(mc_p)_i &= (mc_p)_{EG} + (mc_p)_{s2} + (mc_p)_{s6} + (mc_p)_{NH_3} \\ &= (mc_p)_{EG} + m_s c_{ps6} x\frac{M_{s6}}{M_s} + m_s c_{ps2}(1-x)\frac{M_{s2}}{M_s} \\ &\quad + \rho_{NH_3} V_b \varepsilon c_{pNH_3}\end{aligned} \tag{12}$$

$$\begin{aligned}\varepsilon &= 1 - \frac{V_{EG}}{V_b} - \frac{V_s}{V_b} \\ &= 1 - \frac{\rho_{EG,b}}{\rho_{EG}} - \left[\frac{1-f_{EG}}{f_{EG}}\right][v_{s2} + (v_{s6} - v_{s2})x]\frac{\rho_{EG,b}}{M_s}\end{aligned} \tag{13}$$

The specific heat and the molar volume of the ammoniates (c_{ps2}, c_{ps6} and c_{pEG}, v_{s2} and v_{s6}) were presented by Han et al. [15]. Intensive research effort on the graphite-salt compounds has proven expanded graphite enhancing the heat and mass transfer properties of the sorbent blocks as well as avoiding salt agglomeration. The optimal mass ratio and the preferable conditions have been identified to operate the chemisorption without the heat- and mass-transfer limitation concerns [15,17,20–23]. In order to optimise the performance and simplify the numerical modelling thereby more focus on the combination of adsorption and expander, the mass fraction of the EG (f_{EG}) and the bulk density of the compound were chosen in this work as 0.6 and 400 kg/m^3, respectively. Hereby, because of the high thermal conductivity of the graphite matrix and non-noticeable influence of the heat transfer coefficient at the wall on the global transformation with the given mass ratio and density, heat-transfer limitation has been reasonably neglected [15,21]. Since only decomposition process has been studied, where the constraint pressure is too high (>15 bar) to be evidently influenced by permeability and to further pose any mass-transfer difficulty [17,21], non-mass-transfer-limitation assumption has been taken. The physical model could be imaged as stainless steel cylinders containing thin layer reactant with a thickness of 15 mm (δ_r). The mass amount of the salt used should be adjusted and determined to satisfy the expansion performance for the expected power output.

3.1.3. Adsorption model verification

As Fig. 4 showing the comparison between the experimental data from the work done by Lu and Mazet [21] and the simulated results in this work under the same conditions, there are good agreement during the period of the first 15–20 min which was exactly cyclic operation time discussed in this work, otherwise the specific cooling power (SCP) would be severely compromised. The growing deviation with the time length and the conversion evolvement could be explained as: the experimental data was from synthesis where the heat- and mass-transfer limitation should be taken into account mainly because of the low working pressure; whereas, the presented model was engaging with decomposition where the favourable operation conditions as discussed before, heat- and mass-transfer limitation could be ignored. Therefore,

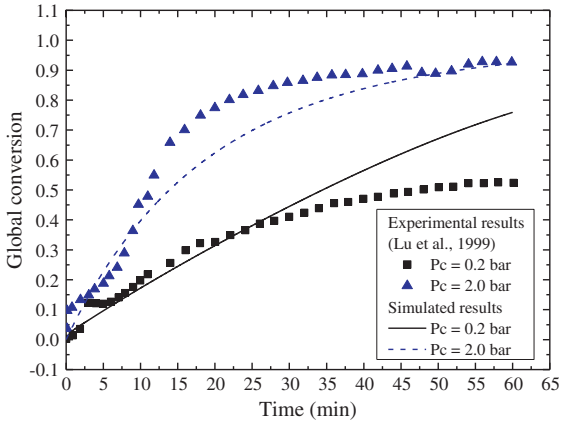

Fig. 4. Comparison of the experimental data and simulation results on adsorption cycle.

the presented model can be concluded as reliable in accordance with the specific operation conditions in this work.

3.2. Scroll expander model

Table 1 summarises the parameters involved in the scroll expander modelling.

3.2.1. Volume equation

The volume of the suction chamber can be calculated by the following equation [24,25]:

$$V_1 = (2S_{11} - S_{12} - 2S_{13})H \tag{14}$$

where S_{11}, S_{12} and S_{13} are expressed as follows:

$$S_{11} = \frac{1}{6}r^2\left[\left(\theta + \frac{1}{2}\pi - \alpha\right)^3 - \left(\theta - \frac{1}{2}\pi - \alpha\right)^3\right] \tag{15}$$

$$S_{12} = r^2(\pi - 4\alpha) \quad R_{or} \geq 2r \tag{16}$$

$$S_{12} = r^2\left\{\pi - 4\alpha + \arccos\left(\frac{\pi}{2} - \alpha\right) - \left(\pi - 2\alpha\right)\sin\left[\arccos\left(\frac{\pi}{2} - \alpha\right)\right]\right\} \; R_{or} \leq 2r \tag{17}$$

$$S_{13} = r^2\alpha\left(\theta - \frac{\pi}{2}\right) + \frac{1}{3}r^2\alpha^3 \tag{18}$$

For other chambers, the volume equation is given as [24,25]:

$$V_i = \pi P_{it}(P_{it} - 2t)\left(\frac{\theta}{\pi} + 2i - 3\right)H \tag{19}$$

where i is the chamber number counting from suction chamber to exhaust chamber.

3.2.2. Mass equation

In the Ad-Cogen system, the inlet mass flow rate of the expander was determined by the desorbed ammonia rate of the chemisorption cycle. However, the former one was not necessary always equal to the latter one, because practically the dominant factor is the inlet pressure of the expander: the quantity of the ammonia that could pass through the expander is restricted by the maximum limit of the pressure inside the suction chamber, which would never ever exceed the released ammonia pressure at the inlet of the expander. In order to create a comparative atmosphere between the individual and cogeneration performance, a set of flow rates were given as an initial condition and at the same time as the maximum limit value. Thereafter the algorithm of the present model handled this by two options: if the inlet flow rate is acceptable by the pressure limit then the mass flow rate of the expander is equal to the given value (individual mode) or the desorption rate (Ad-Cogen mode); otherwise the flow rate would be iterated until it is admissible.

Table 1
Parameters for scroll expander modelling.

Parameter	Value
Number of chambers	3
Basic circle radius (r)	2×10^{-3} m
Scroll pitch (P_{it} (=$2\pi r$))	1.257×10^{-2} m
Orbiting radius (R_{or} (=$P_{it}/2 - t_w$))	4.083×10^{-3} m
Wrap thickness (t_w)	2.2×10^{-3} m
Wrap height (H)	3×10^{-2} m
Initial angle of involute ($\alpha = t_w/2/r$)	0.55
Axial, radial clearance (C_a, C_r)	1×10^{-4} m
Axial, radial flow coefficient (f_a, f_r)	0.9

The quantity of working gas inside the chambers can be calculated based on the mass balance:

$$\frac{dm_i}{dt} = \dot{m}_{in} - \dot{m}_{out} \tag{20}$$

The leakage between chambers composes the radial leakage and the axial leakage. The former leakage is caused by the gap between the scroll wrap and the bottom plate, while the latter one is caused by the gap between the scroll wraps. The equations for radial and axial leakages are given as follows [26]:

$$\frac{dm_{a,i}}{dt} = f_a C_a L_{a,i}\left[\frac{2k}{k-1}P_i\rho_i\left(\varepsilon'^{\frac{2}{k}} - \varepsilon'^{\frac{k+1}{k}}\right)\right]^{1/2} \tag{21}$$

$$\frac{dm_{r,i}}{dt} = 2f_r C_r H\left[\frac{2k}{k-1}P_i\rho_i\left(\varepsilon'^{\frac{2}{k}} - \varepsilon'^{\frac{k+1}{k}}\right)\right]^{1/2} \tag{22}$$

where $L_{a,i}$ is the axial clearance length, described as following equation:

$$L_{a,i} = 2\pi r[2\pi(i-1) + \theta] \tag{23}$$

The pressure ratio, ε', is:

$$\varepsilon' = \frac{P_{i+1}}{P_i}, \quad \frac{P_{i+1}}{P_i} \geqslant \left(\frac{2}{k+1}\right)^{\frac{k}{k-1}} \tag{24}$$

$$\varepsilon' = \left(\frac{2}{k+1}\right)^{\frac{k}{k-1}}, \quad \frac{P_{i+1}}{P_i} < \left(\frac{2}{k+1}\right)^{\frac{k}{k-1}} \tag{25}$$

3.2.3. Temperature and pressure equations

The temperature and pressure of the working fluid at the inlet of the expander were determined by the heat source and the corresponding equilibrium pressure of the decomposition. Meanwhile, the back pressure of the expander was the pressure in the downstream condenser.

The temperature of the working fluid inside the expanding chamber can be calculated based on the changing volume, the flow rate and the properties of the inlet and outlet working fluid, as described by the following equation [27]:

$$\frac{dT_i}{dt} = \frac{\dot{m}_{in}h_{in}/V_i - \dot{m}_{out}h_i/V_i - [X]\widehat{h}_i(dV_i/dt)/V_i - (d[X]/dt)\widehat{h}_i + P_i(d[X]/dt)/[X]}{[X]c_p - P_i/T_i} \tag{26}$$

where $[X]$ is the molar volumetric concentration and $\widehat{h}$ represents the specific enthalpy on a molar basis, as being derived as follows:

$$[X] = n/V \tag{27}$$

$$\widehat{h} = mh/n \tag{28}$$

The pressure in the chambers was then calculated on the basis of the changing volume, temperature and mass by the following equation [27]:

$$\frac{dP_i}{dt} = \frac{1}{V_i}\left(\frac{dm_i/dt}{M}R_C T_i + R_C\frac{dT_i}{dt}\frac{m_i}{M} - P_i\frac{dV_i}{dt}\right) \tag{29}$$

3.2.4. Motion equation

The rotation of the expander is driven by the force generated by the pressure differences between the chambers. Driving force in each chamber can be calculated by the following equation [24,25]:

$$F_{t,i} = P_{it}H\left[2(i-1) + \frac{\theta}{\pi}\right](P_i - P_{i+1}) \tag{30}$$

Then, the driving torque can be calculated by Eq. (31) [24,28,29]:

$$M_t = R_{or}F_t = R_{or}\sum F_{t,i} \tag{31}$$

Taking the frictions and the rotation load into consideration, and based on Newton's second law of angular motion, the motion dynamics of scroll expander can be described by [25,27]:

$$(J_s + J_L)\frac{d\omega}{dt} = M_t - (k_s + k_L)\omega - T_L \tag{32}$$

For a DC generator connected to the expander as a load, the torque, T_L, that caused by the electricity generation is given as [27]:

$$T_L = k_t I_{ar} \tag{33}$$

$$\frac{dI_{ar}}{dt} = \frac{k_e}{L_{ar}}\omega - \frac{R_{ar} + R_{ar,L}}{L_{ar}}I_{ar} \tag{34}$$

3.2.5. Power equation

The technical power that generated by the expansion and the output shaft power can be calculated by the following equations [27]:

$$\text{Power}_{tec} = -\sum\left(V_i\frac{dP_i}{dt}\right) \tag{35}$$

$$\text{Power}_{shaft} = M_t\omega \tag{36}$$

Then the mechanical efficiency of the scroll expander is defined as:

$$\eta_{mech} = \frac{\text{Power}_{shaft}}{\text{Power}_{tec}} \tag{37}$$

3.2.6. Expander model verification

The expander model was validated by two sets of experimental data of two scroll expanders with different dimensions, one was reported by Liu et al. [26] and the other from the authors' own tests, as shown in Fig. 5. With the lack of manufactural specification, some variables cannot be easily determined, like the leakage clearances (C_a, C_r) and the flow coefficients (f_a, f_r) in Eqs. (21) and (22), neither the friction coefficients (k_s, k_L) in Eq. (32) which is influential on the simulation performance. In this work, the former two variables were reasonably selected based on previous works [27,30]; however, the friction coefficients of the scroll and the load which has been barely reported in published papers, was adjusted at a reasonable range to match the experimental results. The comparison between the simulation and experiments suggested a certain set of values acceptable. The test bench the authors have tested had a generator attached with the expander through magnetic coupling, and because of the minimum rotation speed limitation of the generator, some degree of discrepancy between simulation and experiments was expected at low speeds as can be seen in Fig. 5.

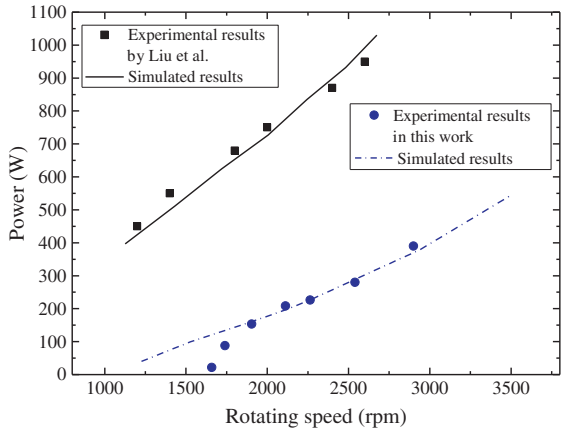

Fig. 5. Comparison of the experimental data and simulation results on scroll expander.

3.3. Performance analysis methods

The exhausted refrigerant gas from the expander was condensed and liquefied in condenser, thereafter the liquid refrigerant evaporated as the synthesis occurring in the Ad-Bed, thus the refrigeration is obtained. To simplify the analysis from the perspective of a general comparison, all refrigerant released by the decomposition was ideally assumed to be reversibly transferred and fully adsorbed in the following sequential synthesis process. Then, the system refrigeration COP, thermal efficiency η_{therm}, and the exergy efficiency η_{ex} of the cogeneration can be calculated by:

$$\text{COP}_{ref} = \frac{Q_{ref}}{Q_{heat}} \tag{38}$$

$$\eta_{therm} = \frac{W + Q_{ref}}{Q_{heat}} \tag{39}$$

$$dE_{heat} = dQ_{heat}\left(1 - \frac{T_0}{T_{de}(t)}\right) \tag{40}$$

$$dE_{ref} = dQ_{ref}\left(\frac{T_0}{T_{ref}(t)} - 1\right) \tag{41}$$

$$\eta_{ex,ref} = \frac{E_{ref}}{E_{heat}} \tag{42}$$

$$\eta_{ex,power} = \frac{W}{E_{heat}} \tag{43}$$

Q_{ref} represents the refrigerant vaporisation heat, W means the work output by the scroll expander, and Q_{heat} is the input thermal energy. E_{heat} and E_{ref} represent the exergy of the input heating energy and the refrigeration product, respectively.

4. Results and discussions

4.1. Individual performance

4.1.1. Expander results

Figs. 6 and 7 show the dynamics variables of pressure and temperature in different chambers of the scroll expander under a typical chosen condition. As shown in the figures, stabilisation of the output only took less than 0.1 s. The ammonia flow gained a pressure drop around 1.4 MPa with the expansion ratio around 3.19 by passing through the expander that studied in this work, as well as a temperature decrease about 75 °C.

With the given backpressure, the higher inlet temperature (the inlet pressure is the corresponding equilibrium pressure of the decomposition) or the higher flow rate of the supplying ammonia to the expander resulted in the higher rotating speed and eventually more power output. Nevertheless, the power output was subjected to the collective influence of the inlet temperature and the flow rate. These two variables interacted with each other on their impacts on the expander performance. Fig. 8 illustrates the developing trend of the expander performance in terms of the shaft power output and the mechanical efficiency under different conditions. Both the power output and the mechanical efficiency increased with the increasing flow rate, but they eventually halted at certain points and thereafter remained constant irrespective of

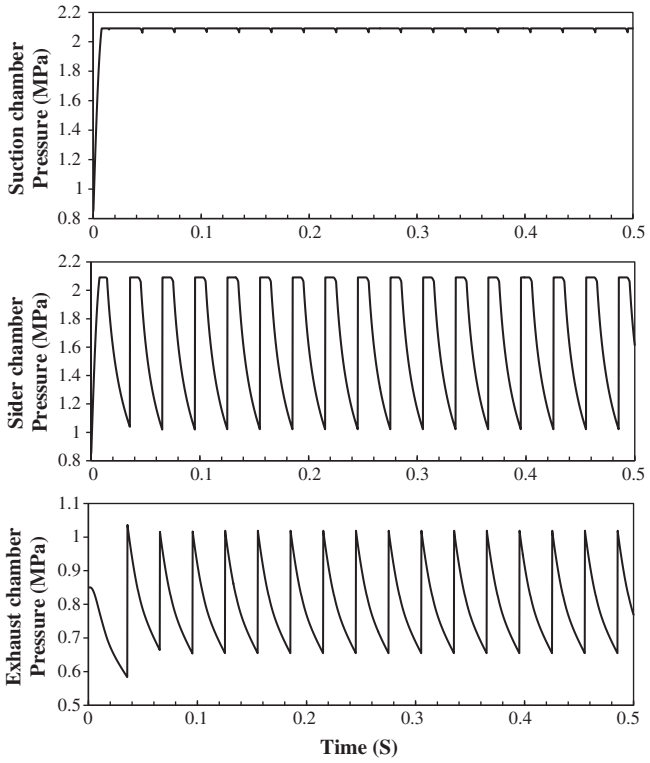

Fig. 6. Chamber pressure variation with 170 °C inlet temperature, 2.1 MPa inlet pressure and the maximum flow rate of 0.01 kg/s.

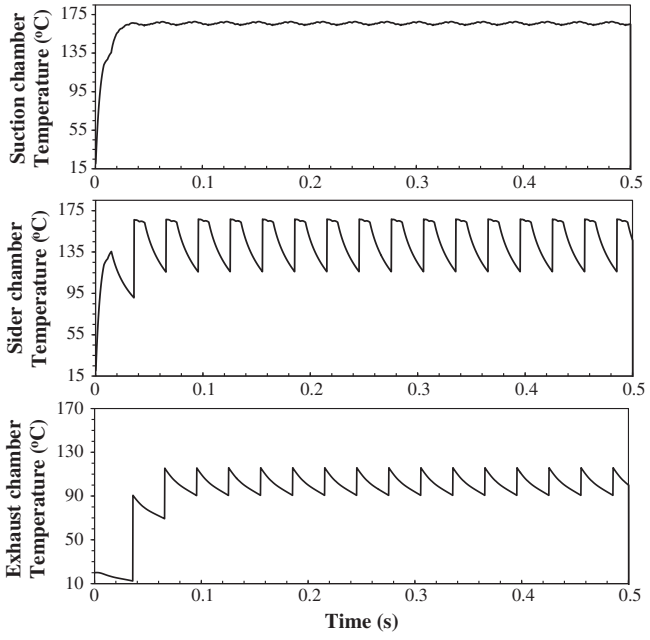

Fig. 7. Chamber temperature variation with 170 °C inlet temperature, 2.1 MPa inlet pressure and the maximum flow rate of 0.01 kg/s.

the increment in the flow rate. The cause of this was that there was an upper limit for the inlet flow rate at a certain inlet pressure, since the pressure of the suction expander chamber could not exceed the inlet vapour pressure as aforementioned. At low flow rate, the raise of the inlet temperature introduced inconspicuous increase in both power output and the mechanical efficiency, whereas at the given flow rate higher than 0.01 kg/s the gap

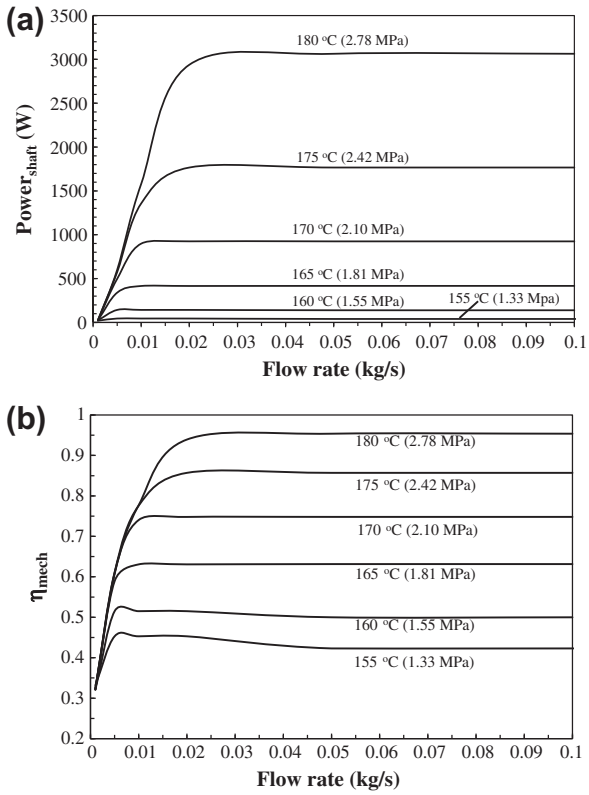

Fig. 8. (a) Shaft power generation and (b) mechanical efficiency of scroll expander varying with different conditions of the flow rate and the inlet pressure and temperature of the ammonia.

between each other performance under different inlet temperatures became more distinct. In this instance, it can be predicated that continuously increasing the inlet temperature can create the opportunity to break through the performance, on the basis of the tendency presented by the currently available data.

To target around 1000 W electric power output, the preferable operating condition of 170 °C inlet temperature and 0.01 kg/s flow rate of the ammonia vapour, which could achieve 925 W shaft power output (Fig. 8), was identified, and the mechanical efficiency of expander could obtain as high as 0.74.

4.1.2. Desorption results

In a single adsorption cycle, the constraining pressure imposed on the adsorbent compound is the saturated pressure of the ammonia inside the condenser during the decomposition, and it switches to the evaporator during the synthesis. The distance between the constrained state and the thermodynamic equilibrium state of the salt complex refers to the equilibrium drop, which is the driving force of the chemical reaction and that dominantly determines the reaction rate. Therefore, the decomposition rate can be speeded by increasing the equilibrium drop, meanwhile the time duration of the reaction can also be shortened. The evolvement of the reaction conversion and the decomposition rate versus the time are shown in Figs. 9 and 10, respectively, with different heat resource temperatures.

Figs. 9 and 10 are plotted on the premise of the fixed heat sink temperature of 20 °C in the condenser and the initial temperature of the adsorbent compound at 140 °C, which is the threshold state of the decomposition of $MnCl_2$ complex corresponding to the constraining pressure in the condenser. This initial condition can be realised by isolating the adsorbent bed from the condenser until the temperature of the former one being heated up to 140 °C.

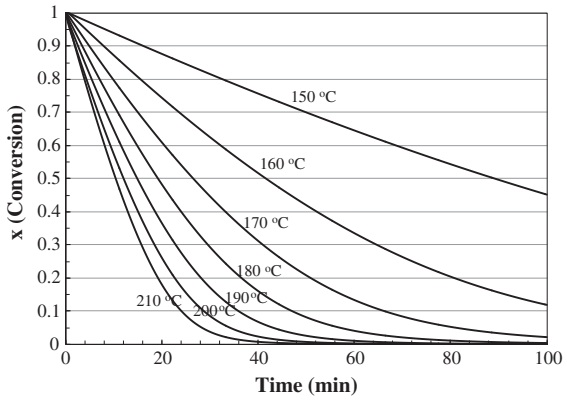

Fig. 9. Reaction conversion variation with different heating temperature during decomposition at 20 °C condensation temperature.

The higher heat source provides the larger equilibrium drop, resulting into the faster reaction rate, consequently the steeper dropping of the reaction conversion in Fig. 9 and the more pointed peak value of the released gas flow rate at the beginning of the process as shown in Fig. 10.

Since it was aimed to meet the demand of 1000 W power generation throughout 15-min time length of the ammonia supply, the numerical modelling were adjusted to identify the optimal operating condition of the desorption and the quantity of adsorbent compound required for sufficient supply. As a result, the composited adsorbent should comprise with 330 mol (41.53 kg) of $MnCl_2$ salt and the 62.3 kg expanded graphite which weights 60% of the compound. As shown in the figures, based on the estimation that the temperature difference between the heat source and the adsorbent bed was 10 °C, the decomposition with 180 °C heating temperature could sufficiently feed the expander with the working fluid at an average flow rate of 0.01 kg/s at the inlet temperature around 170 °C, which meets the aforementioned requirement of power generation. The global conversion achieved 40% for 15 min desorption process.

4.2. Cogeneration performance

In cogeneration cycle, adsorbent bed, the scroll expander and the condenser were linked in series. The constraining pressure imposed on the decomposition is the pressure inside the suction chamber of the expander instead of the saturated pressure inside the condenser.

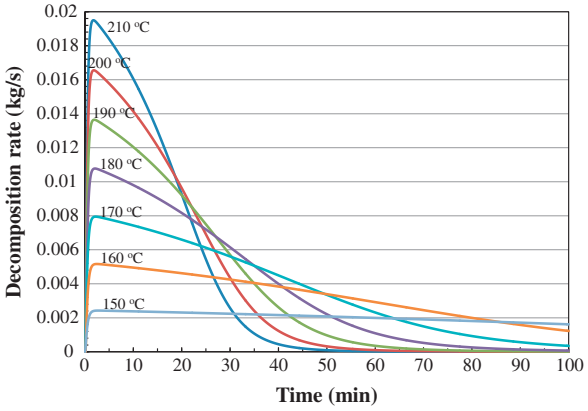

Fig. 10. Decomposition rate variation with different heating temperature during decomposition with 20 °C condensation temperature.

Fig. 11 shows the comparison of the working fluid flow rate between desorption-only mode and cogeneration mode, as well as that of equilibrium pressure drop of the decomposition. Comparing to the desorption-only mode, the additional existence of the expander in the downstream position inhibited the development of the chemical reaction to certain extent, because the operation of expander would consume part of the pressure difference between the decomposition and the condensation. Therefore the equilibrium pressure drop reduced in cogeneration mode, e.g. decreasing from about 5 MPa to 3 MPa at 180 °C heating temperature. As a consequence, the decomposition rate declined.

Typical decomposition rate reduction caused by the expander is shown in Fig. 12. The expander fed on the unstable flow rate of the ammonia, due to the distinct chemical kinetic characteristics of the chemisorption. There is a striking contrast of the flow rate between the two modes, and it is palpable that the decomposition rate of the cogeneration mode 'Cogen (i140-h180)' features the combined characteristics of the chemical kinetic and the rotary kinetic, and it is lower than that of desorption-only mode 'Des (i140-h180)'. This reduction reflects the mutual restricting effect between desorption and expansion in cogeneration mode. With the condition of heating temperature at 180 °C, the average value of the flow rate of 'Cogen (i140-h180)' was about 57.7% smaller than that of 'Des (i140-h180)', while the best case is the former one around 47% smaller

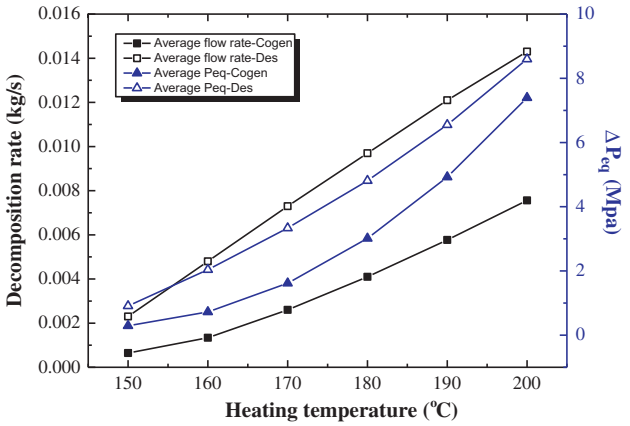

Fig. 11. Average decomposition rate and equilibrium pressure drop with different heating temperature.

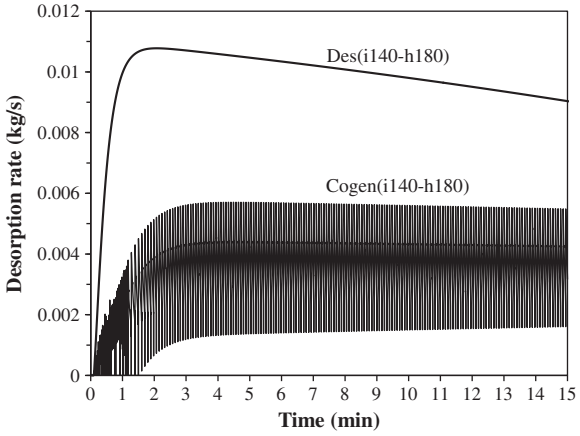

Fig. 12. Decomposition rate of cogeneration mode compared with desorption-only mode.

than the latter one at heating temperature 200 °C and the worst case was around 72% smaller at 150 °C heating temperature.

The cogeneration performance was sensitive to the increase in heat source temperature, as shown in Fig. 13, because the heating temperature significantly affected the decomposition which was also responsible for the inlet temperature and mass flow rate of the expander. The higher heat source temperature was, the stronger the driving force of the decomposition became, thus the decomposition rate of the working fluid would increase consequently. Meanwhile, the temperature of the vapour heading to the expander would also corresponding raise. As a result of the collective effort of the increasing flow rate and the increasing inlet temperature, the benefit was multiplied, i.e. the growth of the power output displayed in Fig. 13 is accelerating.

It can be observed that after two to three minutes stabilisation of the expander at the beginning, the decomposition rate of 'Cogen (i140-h180)' evolved with regular frequency in Fig. 12. Since the relatively stable flow rate appeared, the output power curve became relatively flat and stable around the peak value (Fig. 13). However the performance at 180 °C heating temperature only achieved around 320 W power output, just one third of the original expectation by simulating the two processes separately under the same conditions, which is shown in Fig. 8 as about 925 W. But when the heat source temperature was up to 200 °C, the cogeneration mode could yield the average power output around 900 W.

The combination of desorption and expansion cannot be treated as simple superposition of the processes, the interaction between them is mutual negative restriction, especially for the chemisorption cycle that possesses distinct chemical kinetics. This mutual impact was the main reason why the cogeneration mode gained lower power output than the initial expectation by calculating the simple sum effect of the individual performance of the chemisorption and the expansion. Chemisorption requires as low downstream pressure as possible, while the expansion expects higher feeding pressure. This becomes contradictory and compromises the overall performance when these two cycles link in a series loop and they share the same pressure point but different requirements. There is always a balance proceeding between these two cycles in every second during the whole 15 min desorption.

Therefore, it leads to a key subject to maximise the performance: the selection and matching work between the adsorption system and the expander. The flow rate and the thermal properties of the supplying working fluid generated by desorption cycle affect the expansion performance significantly which is also adversely affecting the desorption. In the case of dis-match between these two, vicious circles would occur regardless of either one is not satisfactory for the other one. If the decomposition rate of the working fluid exceeds the maximum inlet of the expander, then more and more working fluid could not pass through the expander but remain in the adsorbent bed. And that would increase the constraining pressure of the decomposition and prevent the further proceeding, leading to the lowering decomposition rate. The smaller the decomposition rate is, the slower the expander can rotate. Thus the even less working fluid could pass through. On the other hand, if the expander needs larger flow rate, the size of the metallic itself is correspondingly bigger and that requires stronger input to provide sufficient torque for itself rotation and simultaneous power output. In this instance if the desorption could not offer the working fluid at the matched level of the flow rate, there would be no proper rotation and lead to poor power output.

Nevertheless, with a given expander and the same temperature heat source, merely multiplying the scale of the desorption system and expecting higher flow rate from desorption would not assure an equally proportional increase in the cogeneration performance. This delusion overlooks again the interaction between the two processes. As Fig. 8(a) indicating the inlet limit of the expander, for any one fixed temperature heat source, there is a peak value point that the power output would stable at regardless of the continuously increasing flow rate. That is restrained by the specific dimension of the expander. For example, even if the adsorbent bed in Ad-Cogen system simulated in this work is scaled up to 5 times larger but still employing the same heat source at 180 °C, the power output cannot reach more than 520 W. In this instance lifting the heat source temperature would be more viable and more effective, but this involves other considerations, such as more input energy would be needed and the optimal point of it need to be identified in order to maximum the thermal efficiency.

It is also worth noting that the specific geometric dimension parameters of the scroll expander are equally influential in both individual performance and matching work. According to the experience in this work when adjusting these parameters in the simulation, even small changes of those could cause surprising consequences in performance. Deliberately and precisely setting up each dimension parameter would effectively improve performance. Since the expander design is beyond the main scope of this work, this subject would not be extended to details here.

Finally, taking the condition (i140-h180) as an example, the performance was roughly compared between the two modes within 15 min reaction time in terms of COP and thermal efficiency for −10 °C refrigeration, respectively. In desorption-only mode, COP_{ref} was around 0.339 with the cyclic conversion about 0.39. It is 65% higher than what the cogeneration mode could achieve which

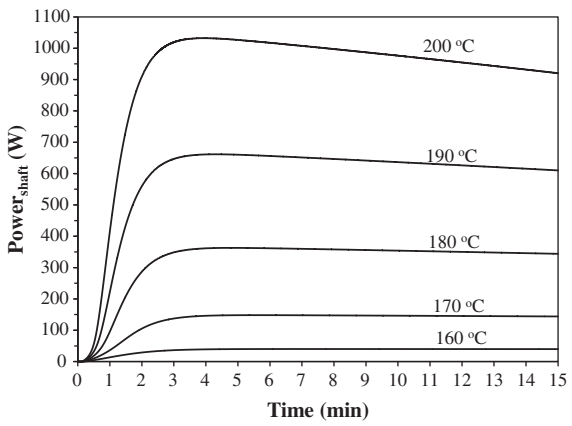

Fig. 13. Power output with different heating temperature in Ad-Cogen system.

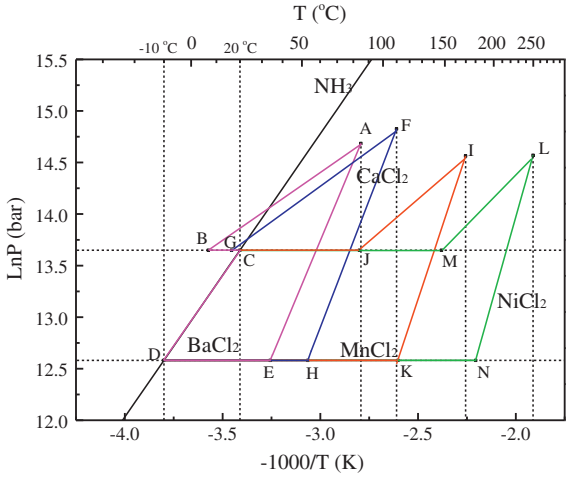

Fig. 14. Thermodynamic cycle of the cogeneration system with four different salt complexes.

Table 2
The performance of different salt complexes used in ideal cogeneration cycle.

Salt complexes	Desorption temperature (°C)	Desorption pressure (MPa)	Reaction enthalpy ΔH_r (J/mol(NH_3))	COP	Exergy efficiency	
					Power	Refrigeration
$BaCl_2$ (8–0 NH_3)	85	2.4	37665	0.57	0.39	0.23
$CaCl_2$ (8–4 NH_3)	106	2.4	41013	0.41	0.24	0.13
$MnCl_2$ (6–2 NH_3)	175	2.4	47416	0.42	0.19	0.089
$NiCl_2$ (6–2 NH_3)	255	2.4	56160	0.34	0.14	0.056

was about 0.206 due to the small conversion around 0.14. Apart from the refrigeration output, the cogeneration mode had simultaneous work output which represents the higher grade energy and could account for extra 0.025 contributing to the thermal efficiency in Eq. (39).

Compared with APC system which has a pressure difference between the inlet and outlet of the expander around 7–11 MPa [9,10] which is suitable for medium scale power plant. The maximum value of that in Ad-Cogen system in this work was no more than 2 MPa and that is partially the reason the scroll expander being chosen over the turbine, and it was aimed to apply to small scale household standalone system.

The methodology that other absorption cogeneration works have being discussing, is usually firstly to calculate the enthalpy difference of the working fluid as it passing through the expander, and thus to obtain the result of the final net work by multiplying the enthalpy difference with an empirical value of an isentropic efficiency. If such an approach is applied to the Ad-Cogen system in this work, it could expect a net work output accounting for 0.13 of thermal efficiency. However, more realistic modelling of the scroll expander was studied in this work, more dynamic factors involved not just in the expander but also in the complex chemisorption cycle have been considered.

4.3. Adsorbent salts selection

Because of the virtues of the innumerable candidates for adsorption cycle, a part of the optimisation effort can be engaged with the selection of the reactive salt complexes. Fig. 14 illustrates the ideal thermodynamic cycles of the cogeneration system with four different salt complexes in Clausius–Clapeyron diagram, they are $BaCl_2$ (cycle ABCDEA in Fig. 14), $CaCl_2$ (FGCDHF), $MnCl_2$ (IJCDKI) and $NiCl_2$ (LMCDNL) respectively in a low-to-high order of decomposition temperature at the same working pressure. The performance of these salts was compared on the basis of the same amount of the ammonia cyclic transferring and the conditions of the heat sink at 20 °C and the refrigeration at −10 °C. The energy and exergy efficiency of each cycle were evaluated by Eqs. (38)–(43) and summarised in Table 2.

The cycle with $BaCl_2$ ideally offered the highest COP and exergy efficiency amongst all. Observing from the Clapeyron diagram, the one that has an equilibrium line closer to the saturated line of ammonia can be driven by the lower heat source but provide higher pressure of vapour ammonia, therefore it leads to the improvement of the energy and exergy efficiency. Thus, the salt complexes $BaCl_2$ and $CaCl_2$ are theoretically more preferable than $MnCl_2$ studied in this work. Beyond the former two there is a great deal of potential salt complexes can be taken into consideration, however, there is still an optimal point of the cogeneration performance. If the equilibrium line of the salt complex is too close to the ammonia line, the performance of synthesis related with the evaporation refrigeration would be compromised, because of insufficient pressure difference.

Therefore, the following reasons are summed up for the relatively low power output in this work, (1) a small-scale cogeneration unit was discussed and that is also the purpose choosing the scroll expander in this work, however a turbine would be more applicable for medium scale power plant; (2) differing from the absorption, the more complex chemisorption involving the coupling of thermodynamic and chemical kinetics is naturally unable to generate stable working fluid at a constant flow rate, which would affect the expander performance and further influence the global performance; (3) the mutual constraint between the chemisorption process and the expansion process, and the dis-match between them, is one of the dominant causes; and (4) elaborately selecting the adsorbent salt complex would be helpful to improve the performance.

5. Conclusion

The novel combination of the chemisorption cycle and the scroll expander for refrigeration and power cogeneration, which is promisingly coping with the globally concerned issues of the scarce energy and the global warming, has been for the first time investigated with numerical simulation model in this work. Driven by low grade heat, this concept with two sets of chemisorption cycle working out-of-phase can realise cooling and electricity continuous and simultaneous generation.

With the aid of the validated numerical modelling, performance evaluation of the Ad-Cogen system was carried out. It was found that under the same heat source condition, the performance of the cogeneration mode was inferior to the simple sum of the individual performance of the adsorption part plus the expansion part, which only generated about 320 W power compared to the expected value around 1000 W. It was mainly because of the strong mutual constraint between them, which was partially attributed to the dis-match between the adsorption part and the expansion part and non-optimal dimension design of the scroll expander. The compromise between them reduced the global performance. Alternatively, with the given expander, increasing the heat source temperature and if necessary at the same time scaling up the chemisorption part in order to achieve better match is potential to optimise the global performance. Moreover, there are various potential candidates of reactive salt complexes readily for the improvement of the Ad-Cogen system.

The viability of the Ad-Cogen system as a refrigeration-and-electricity cogeneration system was simulated and demonstrated. Considering the tremendous potential of Ad-Cogen system addressing all the energy, environmental and economic issues those have been encountered by the conventional refrigeration and power generation technologies, more fundamental research and the essential exploration urges more effort to guide the practical system design and the optimisation work, thus to further validate and extend the application of the Ad-Cogen system.

Acknowledgement

The authors gratefully acknowledge the support from the Engineering and Physical Sciences Research Council projects (EP/I027904/1and EP/K004689/1) of UK.

References

[1] Digest of UK energy statistics, 2012.
[2] Kassakian JG, Schmalensee R, etc. The future of the electric grid. An interdisciplinary MIT study. December 5, 2011 http://mitei.mit.edu/publications/reports-studies/future-electric-grid.
[3] Climate change act, 2008.
[4] McHenry MP. Small-scale ($\leqslant$6 kW_e) stand-alone and grid-connected photovoltaic, wind, hydroelectric, biodiesel, and wood gasification system's simulated technical, economic, and mitigation analysis for rural regions in Western Australia. Renew Energy 2012;38:195–205.
[5] Technical manual: BREEAM-NOR ver. 1.0 (2012). ASHRAE position document on ammonia as refrigerant, 2006.
[6] Goswami DY. Solar thermal power-status of technologies and opportunities for research. In: Proceedings of the second ISHMT-ASME heat and mass transfer conference, New Delhi: Tata McGraw Hill, Suratkal, India, 1995.
[7] Hasan AA, Goswami DY, Vijayaraghavan S. First and second law analysis of a new power and refrigeration thermodynamic cycle using a solar heat source. Sol Energy 2002;73:385–93.
[8] Tamm G, Goswami DY, Lu S, Hasan AA. Theoretical and experimental investigation of an ammonia–water power and refrigeration thermodynamic cycle. Sol Energy 2004;76:217–28.
[9] Liu M, Zhang N. Proposal and analysis of a novel ammonia–water cycle for power and refrigeration cogeneration. Energy 2007;32:961–70.
[10] Luo CD, Zhang N, Cai RX, Liu M. Sensitivity analysis of ammonia absorption power/refrigeration combined cycle. Proc CSEE 2008;28:1–7.
[11] Wang RZ, Oliveira RG. Adsorption refrigeration – an efficient way to make good use of waste heat and solar energy. Prog Energy Combust Sci 2006;32:424–58.
[12] Fan Y, Luo L, Souyri B. Review of solar sorption refrigeration technologies: development and applications. Renew Sust Energy Rev 2007;11:1758–75.
[13] Spinner B. Ammonia-based thermochemical transformers. Heat Recov Syst CHP 1993;13:301–7.
[14] Wang LW, Ziegler F, Roskilly AP, Wang RZ, Wang YD. A resorption cycle for the cogeneration of electricity and refrigeration. Appl Energy 2013;106:56–64.
[15] Han JH, Lee KH, Kim DH, Kim H. Transformation analysis of thermochemical reactor based on thermophysical properties of graphite-$MnCl_2$ complex. Ind Eng Chem Res 2000;39:4127–39.
[16] Stitou D, Crozat G. Dimensioning nomograms for the design of fixed-bed solid–gas thermochemical reactors with various geometrical configurations. Chem Eng Process 1997;36:45–58.
[17] Lu HB, Mazet N, Spinner B. Modelling of gas–solid reactions coupling of heat and mass transfer with chemical reaction. Chem Eng Sci 1996;51:3829–45.
[18] Oliveira RG, Wang RZ. Study of a non-isothermal, non-isobaric consolidated reactive bed for chemisorption icemakers. Chem Eng J 2008;138:416–24.
[19] Metcalf SJ, Tamainot-Telto Z, Critoph RE. Application of a compact sorption generator to solar refrigeration: case study of Dakar (Senegal). Appl Therm Eng 2011;31:2197–204.
[20] Wang LW, Tamainot-Telto Z, Metcalf SJ, Critoph RE, Wang RZ. Anisotropic thermal conductivity and permeability of compacted expanded natural graphite. Appl Therm Eng 2010;30:1805–11.
[21] Lu HB, Mazet N. Mass-transfer parameters in gas–solid reactive media to identify permeability of IMPEX. AIChE J 1999;45(11):2444–53.
[22] Mauran S, Lebrun M, Prades P, Moreau M, Spinner B, Drapier C. Active composite and its use as reaction medium. US Patent 5283219; 1994.
[23] Oliveira RG, Wang RZ, Wang C. Evaluation of the cooling performance of a consolidated expanded graphite–calcium chloride reactive bed for chemisorption icemaker. Int J Refrig 2007;30:103–12.
[24] Liao DP, Wu YZ. Refrigeration compressor. China Machine Press; 2004.
[25] Chu XG, Zhang CH, Li K, Jing YF. Dynamic modeling and efficiency analysis of the scroll expander generator system for compressed air energy storage. In: International conference on electrical machines and systems (ICEMS), 2011.
[26] Liu GB, Zhao YY, Li LS, Shu PC. Simulation and experiment research on wide ranging working process of scroll expander driven by compressed air. Appl Therm Eng 2010;30:2073–9.
[27] Wang JH, Luo X, Yang L, Shpanin LM, Jia N, Mangan S, Derby JW. Mathematical modeling study of scroll air motors and energy efficiency analysis-Part II. IEEE/ASME Trans Mechatron 2011;16:122–32.
[28] Wang JH, Yang L, Luo X, Mangan S, Derby JW. Mathematical modeling study of scroll air motors and energy efficiency analysis-Part I. IEEE/ASME Trans Mechatron 2011;16:112–21.
[29] Kim H, Kim W, Kim S. Applicability of scroll expander and compressor to an external power engine: conceptual design and performance analysis. Int J Energy Res 2012;36:385–96.
[30] Yang XH, Wang JD, Zhang D. Numerical simulation of a scroll compressor used for compressed air energy storage. In: Computer science and information technology (ICCSIT), Chengdu, China, 3rd IEEE International Conference on, July 2010, vol. 6. pp. 262–66.